



Immune Response to Persistent *Staphylococcus Aureus* Periprosthetic Joint Infection in a Mouse Tibial Implant Model

Upneet K Sokhi,^{1,2}  Yunwei Xia,^{1,2} Branden Sosa,^{1,3} Kathleen Turajane,^{1,3} Sita N Nishtala,^{1,3} Tania Pannellini,^{1,4} Mathias P Bostrom,^{1,3,5} Alberto V Carli,^{1,3} Xu Yang,^{1,3}  and Lionel B Ivashkiv^{1,2,6,7}

¹Research Institute, Hospital for Special Surgery, New York, NY, USA

²David Z. Rosensweig Genomics Research Center, Hospital for Special Surgery, New York, NY, USA

³Arthroplasty Research Laboratory, Hospital for Special Surgery, New York, NY, USA

⁴Department of Pathology, Hospital for Special Surgery, New York, NY, USA

⁵Department of Orthopaedics, Weill Cornell Medicine, New York, NY, USA

⁶Department of Medicine, Weill Cornell Medicine, New York, NY, USA

⁷Immunology and Microbial Pathogenesis Program, Weill Cornell Medicine, New York, NY, USA

ABSTRACT

Staphylococcus aureus is one of the major pathogens in orthopedic periprosthetic joint infection (PJI), a devastating complication of total joint arthroplasty that often results in chronic and persistent infections that are refractory to antibiotics and require surgical interventions. Biofilm formation has been extensively investigated as a reason for persistent infection. The cellular composition, activation status, cytokine profile, and role of the immune response during persistent *S. aureus* PJI are incompletely understood. In this study, we used histology, multiparametric flow cytometry, and gene expression analysis to characterize the immune response in a clinically relevant orthopedic PJI model. We tested the hypothesis that persistent *S. aureus* infection induces feedback mechanisms that suppress immune cell activation, thereby affecting the course of infection. Surprisingly, persistent infection was characterized by strikingly high cytokine gene expression indicative of robust activation of multiple components of innate and adaptive immunity, along with ongoing severe neutrophil-dominated inflammation, in infected joint and bone tissues. Activation and expansion of draining lymph nodes and a bone marrow stress granulopoiesis reaction were also maintained during late phase infection. In parallel, feedback mechanisms involving T-cell inhibitory receptors and exhaustion markers, suppressive cytokines, and regulatory T cells were activated and associated with decreased T-cell proliferation and tissue infiltration during the persistent phase of infection. These results identify the cellular and molecular components of the mouse immune response to persistent *S. aureus* PJI and indicate that neutrophil infiltration, inflammatory cytokine responses, and ongoing lymph node and bone marrow reactions are insufficient to clear infection and that immune effector mechanisms are suppressed by feedback inhibitory pathways. These immune-suppressive mechanisms are associated with diminished T-cell proliferation and tissue infiltration and can be targeted as part of adjuvant immunotherapeutic strategies in combination with debridement of biofilm, antibiotics, and other therapeutic modalities to promote eradication of infection. © 2021 American Society for Bone and Mineral Research (ASBMR).

KEY WORDS: ORTHOPEDICS; OSTEOIMMUNOLOGY; CYTOKINES; BONE INFECTION

Introduction

Orthopedic periprosthetic joint infection (PJI) is a devastating complication that affects 1% to 2% of total joint arthroplasty (TJA) patients per year in the United States.^(1,2) PJI is often not responsive to antibiotic therapy, resulting in debilitating persistent and chronic infections that require invasive interventions, including a combination of debridement, irrigation, and complex revision surgery that involves removal and re-implantation of the

prosthetic implant. One key reason for persistence of PJI is bacterial biofilm that forms on the implant.⁽³⁾ Biofilm is a bacterially produced matrix composed of proteins, extracellular DNA, and polysaccharides that harbors quiescent-phase bacteria that are refractory to antibiotics and shielded from host immune cells. *Staphylococcus aureus* is a major PJI pathogen affecting up to 63% of culture-positive cases⁽⁴⁾ that is often antibiotic-resistant, tissue destructive, and particularly difficult to eradicate.⁽⁵⁻⁸⁾ In addition to forming biofilms, *S. aureus* directly targets innate

Received in original form September 28, 2021; revised form November 22, 2021; accepted December 8, 2021.

Address correspondence to: Lionel B Ivashkiv, MD, Research Institute, Hospital for Special Surgery, 535 East 70th Street, New York, NY 10021, USA.

E-mail: ivashkivl@hss.edu

Additional Supporting Information may be found in the online version of this article.

Journal of Bone and Mineral Research, Vol. 37, No. 3, March 2022, pp 577–594.

DOI: 10.1002/jbmr.4489

© 2021 American Society for Bone and Mineral Research (ASBMR).

and adaptive immune cells to avoid clearance and establish chronic infections.⁽⁹⁻¹¹⁾ A deeper understanding of immune responses against *S. aureus* is essential for the development therapies and vaccines against this pathogen, as efforts to develop effective vaccines have failed.^(12,13)

A primary mechanism of immune defense against extracellular bacteria like *S. aureus* is phagocytosis and killing of microbes by innate immune cells—neutrophils and to a lesser extent macrophages.⁽¹⁴⁾ Influx of neutrophils to sites of infection is mediated by inflammatory cytokines such as IL-1 β and TNF, and by IL-17 family cytokines, that induce chemokine expression and endothelial activation.⁽¹⁵⁾ IL-17 is produced by innate $\gamma\delta$ T cells and by T-helper 17 (Th17) lymphocytes that are part of adaptive immunity. The antimicrobial mechanisms of neutrophils are augmented by inflammatory cytokines, and phagocytic functions are increased by opsonization (coating) of *S. aureus* by complement split products and antibodies, the latter produced by B lymphocytes. The importance of neutrophils, microbicidal mechanisms, signaling by inflammatory cytokines, and type 3 immunity (mediated by IL-17) in anti-Staph immunity is well established, including strong genetic evidence showing loss-of-function mutations in these pathways, specifically in signaling proteins MYD88 and IRAK4 in innate immune cells, and regulators of Th17 cells such as STAT3, in children who are highly susceptible to Staph infections, and by gene deletion studies in mouse models of infection.^(14,16) The current paradigm is that adaptive immunity is important for controlling *S. aureus* infection mainly by increasing the influx and function of neutrophils.^(14,17-19) The inability of combined adaptive and innate immunity to clear *S. aureus* infections is typically attributed to biofilm formation creating an impenetrable physical barrier between the bacteria and host phagocytic cells⁽²⁰⁾ and effective attenuation of immune functions by this bacterium.^(3,9-11,19,21,22) However, affected children outgrow susceptibility to *S. aureus* infections,⁽¹⁶⁾ suggesting either that *S. aureus*-induced suppressive mechanisms can be overcome or that there are alternative immune mechanisms that can clear Staph that are not effectively mobilized during initial infections. Such mechanisms could include macrophage-mediated killing, type 1 IFN- γ -mediated immunity, antibody-mediated phagocytosis, and clearance of intracellular *S. aureus* by CD8⁺ cytotoxic lymphocytes.^(10,23-25) Discovery of immune mechanisms that can clear *S. aureus*, or how to overcome Staph-mediated immune suppression, would offer great promise for developing immunotherapies for *S. aureus* infections.

Staphylococcus aureus suppresses both innate and adaptive immune responses by various mechanisms.^(9,11,21,22) *Staphylococcus aureus* inhibits innate immune responses by producing virulence factors (eg, exotoxins, enterotoxins, adhesive factors) that interfere with opsonization and phagocytosis, suppress neutrophil recruitment and activation by blocking chemoattractants, inhibit killing mechanisms and enzymes, and by producing toxins like leukotoxins and hemolysins that lyse neutrophils and other immune cells.^(26,27) Suppression of adaptive immunity occurs via induction of myeloid-derived suppressor cells (MDSCs, which suppress T-cell proliferation), suppressive cytokines such as IL-10, regulatory T cells (Tregs), and T-cell anergy, a functional state where chronic exposure to antigens renders T cells hyporesponsive to stimulation.^(9,19) Various mouse models of *S. aureus* infection, which include systemic and local infections with or without biofilm, have consistently shown persistent unresolved infection lasting for weeks, with ongoing immune activation locally at the site of infection that is not able to clear the

infection.⁽²⁸⁻³⁸⁾ Thus, in persistent infection, the host and pathogen reach a state of coexistence, where the pathogen is contained by an attenuated immune system and tissue damage is limited, but the pathogen is not eliminated. Regulation of the balance and stability of this equilibrium state is not well understood, but abrogation of key immune-suppressive mechanisms offers the possibility of activating immune responses to help clear infection together with other therapeutic modalities. The promise and potential of such a therapeutic strategy are supported by the immense success of immune checkpoint blockade in activating constrained immune responses to eliminate tumors.^(39,40) In addition to activating cytotoxic lymphocytes that would be effective at targeting infected tissue cells and immune cells such as Trojan horse leukocytes,^(27,41) checkpoint blockade can potentially activate anergic CD4⁺ T cells to mobilize adaptive immunity. However, limitations to an immunotherapy approach are potentially toxicity related to immune overactivation, and that bacteria present in biofilms, whether in *Staphylococcal* abscess communities⁽⁴²⁾ in the soft tissues and bone marrow, in glycocalyx on implants and necrotic tissue, and extracellular bacteria within the canalicular network of the cortical bone, are sequestered from immune cells by an impenetrable barrier.⁽²⁷⁾

Mouse models of orthopedic PJI that faithfully recapitulate acute and also persistent infection that is recalcitrant to antibiotics have been developed by our group and others.^(28,29,35-38,43) These models are characterized by large numbers of MDSCs that can suppress adaptive immunity, but the cellular composition, activation status, and cytokine profile of the immune system at the site of persistent infection have not been well characterized. Even less is known about immune activation status in draining lymph nodes (LNs), where the adaptive immune response initiates, and in bone marrow adjacent to the site of infection. In this study, we tested the hypothesis that persistent *S. aureus* infection activates feedback mechanisms that suppress immune cell activation and cytokine production at the site of infection and also in draining LNs and adjacent bone marrow (BM). We used our recently developed clinically relevant PJI model that incorporates a weight-bearing implant that can osseointegrate, introduction of infection through the same method hypothesized to occur clinically, presence of biofilm on the implant, and progression of infection to intramedullary canal, and enables analysis of both joint soft tissue and bone compartments that are affected by PJI in humans in a mechanically loaded environment.^(28,29) Combined investigation using histology, multiparameter flow cytometry, and gene expression analysis showed that during persistent infection neutrophil infiltration, BM myeloid cell reaction, and innate and adaptive cytokine gene expression remained highly elevated, whereas T-cell proliferation was suppressed in infected tissues and draining LNs and numbers of infiltrating immune cells diminished relative to early stage infection. The late stage was characterized by engagement of feedback mechanisms including increased Tregs and expression of anti-inflammatory IL-10 and increased expression of T-cell inhibitory receptors and exhaustion markers. These results reveal the cellular and molecular components of the mouse immune response to persistent *S. aureus* PJI and indicate that neutrophil infiltration and activation of cytokine responses are insufficient to clear *S. aureus* PJI. The results reveal several immune-suppressive mechanisms that can be targeted as part of immunotherapeutic strategies to promote eradication of infection in combination with other therapeutic modalities.

Materials and Methods

Bacteria

The methicillin-sensitive *S. aureus* strain Xen36 was used in all experiments in this study, as previously described.^(29,43)

Animals, surgical procedures, and treatments

All animal procedures used in this study were approved by the Institutional Animal Care and Use Committee (IACUC) at Hospital for Special Surgery (HSS) and Weill Cornell Medicine (WCM). Nine- to 16-week-old female C57BL/6 mice (Jackson Laboratory, Bar Harbor, ME, USA) were used in all experiments and housed in standard specific pathogen-free (SPF) conditions at the WCM animal facility. A total of 54 mice underwent unilateral proximal tibial implant insertion (right tibia) as described previously.⁽⁴⁴⁾ Specifically, an incision was made in the right knee and the quadriceps fibers divided medially, after which the anterior cruciate ligament and menisci were resected and the patella dislocated to expose the tibial plateau. The tibial articular cartilage and proximal epiphysis were removed with a fine-tip burr. Using a high-speed drill, a 0.9-mm-diameter hole was created in the medullary canal and a 3D printed titanium implant inserted in a press-fit model into the hole, after which the extensor mechanism was closed using resorbable suture and skin closed with non-absorbable suture. Half of the animals ($n = 27$) also received a 2 μ L intra-articular injection of $\sim 10^4$ colony-forming units (CFUs) of *S. aureus* Xen36 after closure of the arthrotomy site.⁽²⁹⁾ Group sizes for each time point and experiment are provided in the figure legends. Accuracy of bacterial dosing at inoculation was confirmed via plating equal amounts of the syringe injections onto kanamycin-containing agar plates in triplicate and counting the colonies after overnight culture. Postoperatively, mice were administered buprenorphine (0.05 mg/kg) every 12 hours subcutaneously for 48 hours and monitored closely as they resumed normal ambulation, which provided mechanical loading onto the implant. For in vivo depletion studies, mice were injected with 250 μ g of anti-CD8 (BioXCell, Lebanon, NH, USA; 2.43, #BE0061) or isotype control (BioXCell, LTF-2, #BE0090) antibodies intraperitoneally (i.p.) starting 2 days before surgery and infection and biweekly after that until euthanasia at 17 days. One mouse died in each group (anti-CD8 and isotype treated) over the course of i.p. injections in the CD8 cell depletion experiment.

Blood collection and ELISA

Animals were euthanized 3, 7, 14, 21, and 35 days after surgery via CO₂ inhalation followed by cervical dislocation and blood was collected via cardiac puncture, from both infected mice and non-infected controls. Blood was collected retro-orbitally on day 28 after mice were anesthetized via isoflurane inhalation. Blood was centrifuged and serum stored at -80°C for future use. Serum amyloid A (SAA) levels were quantified using an ELISA kit (KMA0021; Thermo Fisher Scientific, Waltham, MA, USA) according to the manufacturer's instructions.

Histopathological analysis

Animals were euthanized 3, 7, 14, 21, and 35 days post infection (dpi). Both the operated and contralateral knees including the surrounding musculature from the infected and non-infected animals were fixed in 10% neutral-buffered formalin for 5 to

6 hours. After fixation, bones were demineralized using 10% EDTA after which the implants were gently removed from the tibias with minimal loss of tissue at the bone-implant interface. Tissues were processed using an automated processor (Sakura Finetek, Torrance, CA, USA; VIP 1000) and embedded in paraffin at the HSS histopathology core. Sagittal sections (7 microns thick) of the hind limbs were obtained and stained with hematoxylin and eosin (H&E). Each section included the knee joint and periarticular soft tissues, part of femoral and tibial diaphyses, and surrounding muscles. Histology slides were reviewed by a pathologist at HSS with training in musculoskeletal pathology in a blinded manner. Tissues were scored for histological signs of infection, such as inflammation, abscesses, purulent exudate, and necrosis. The soft tissues were also scored for signs of healing and tissue repair such as fibrosis. Implant osseointegration was estimated by scoring the peri-implant ossification (Supplemental Table S1).

Immunohistochemistry

Paraffin-embedded sections were deparaffinized and rehydrated at the Laboratory of Comparative Pathology at WCM. The sections were stained using the following antibodies: CD3 (Abcam, Cambridge, MA, USA; ab135372, 1:250 after heat-induced epitope retrieval [HIER] in a pH 6.0 buffer); myeloperoxidase (Dako, Glostrup, Denmark; A0398, 1:1000, HIER pH 6.0); and F4/80 (Abcam, ab6640, 1:100, HIER in 10 mM citrate buffer, pH 6.0). Immunohistochemistry was performed on a Leica Bond RX automated stainer using Bond reagents (Leica Biosystems, Buffalo Grove, IL, USA), including a polymer detection system (DS9800, Novocastra Bond Polymer Refine Detection, Leica Biosystems). The chromogen was 3,3-diaminobenzidine tetrachloride (DAB), and sections were counterstained with hematoxylin.

Multicolor flow cytometry

Infected soft tissues surrounding the joint space and implant were harvested and digested with Collagenase A (2.5 mg/mL) and DNase for 15 minutes at 37°C , after which cells were passed through a 70 μ m filter and washed with RPMI. Live/dead cell discrimination was performed using LIVE/DEAD Fixable Dead Cell Stain (Invitrogen, Carlsbad, CA, USA; L23105) according to the manufacturer's instructions followed by subsequent staining with specific antibodies. Bone marrow cells were isolated by centrifugation after cutting the proximal and distal ends of the tibias. Lymph nodes (bilateral iliac and inguinal) were harvested, minced, and digested with type II collagenase (Worthington, Lakewood, NJ, USA) as described.⁽⁴⁵⁾ Single-cell suspensions were counted and then incubated with purified rat anti-mouse CD16/CD32 (mouse Fc block; BD Biosciences, San Jose, CA, USA; #553141 used at 1:50 dilution) before proceeding to surface marker staining. The following fluorophore-conjugated antibodies were used: anti-CD3, CD4, CD8, CD25, CD69, NK1.1, TCR $\gamma\delta$, CXCR5, ICOS, CD11b, F4/80, Ly6C, Ly6G, CD11c, I-Ab, CCR2, and CD9 (additional information provided in Supplemental Table S2). The Foxp3/Transcription Factor staining buffer set (Thermo Fisher Scientific) was used to fix and permeabilize cells for intracellular staining of Foxp3 and Ki67. Cells were analyzed on a FACS Canto (BD Biosciences) according to the manufacturer's guidelines. Data were analyzed with FlowJo v10 software. Total cell populations per lymph node were calculated by multiplying the percentage of gated population by the lymph node cell count. Uniform manifold approximation and projection

(UMAP) analysis was performed on the flow cytometry data sets using the following parameters in FlowJo: nn (nearest neighbors) = number of colors, min_dist of 0.0001 and Euclidean distance.

RNA isolation

All samples, ie, soft tissue, cancellous bone, and peri-implant tissue from the infected and non-infected control mice, were

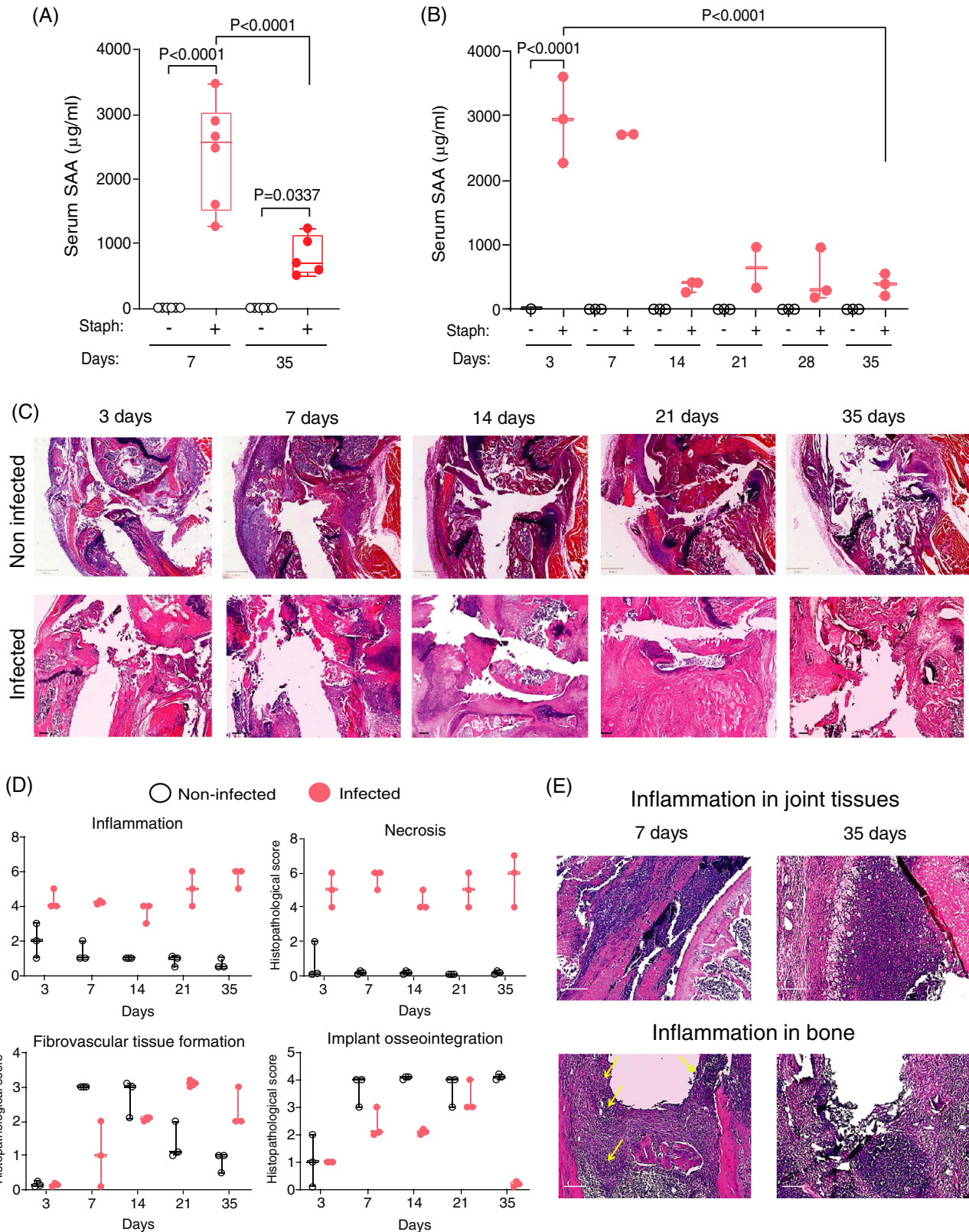


Fig. 1. Legend on next page.

dissected and flash-frozen separately in liquid nitrogen. Soft tissue and cancellous bone samples were harvested bilaterally, ie, from the operated right side (R) and the non-operated left side (L) from the infected (+) and non-infected groups (–). Samples were mechanically homogenized in TRIzol (Invitrogen) and total RNA was extracted using the RNeasy Mini kit (Qiagen, Valencia, CA, USA) following the manufacturers' instructions.

Real-time quantitative polymerase chain reactions (RT-qPCR)

cDNA was synthesized using the RevertAid First Strand cDNA Synthesis Kit (Thermo Fisher Scientific) and real-time qRT-PCR was performed using Fast SYBR Green Master Mix and an ABI7500 Fast system (Applied Biosystems). Gene expression was normalized to mouse *Hprt* and calculated using the $\Delta\Delta Ct$ method. Gene-specific primer sequences used are listed in Supplemental Table S3. Heatmaps for expression of specific genes were generated using ΔCt values and colors were scaled by row (Z scores); data represent average values of 3 to 6 mice per group.

Statistics

Graphs in the figures are presented as a median, interquartile range and the number of mice (*n*) per group. Statistical analyses were performed with GraphPad Prism 8 for Windows (GraphPad Software, Inc., La Jolla, CA, USA). No animals were excluded from the analysis. All data were tested for normality using the Shapiro–Wilk normality test. Student's *t* test and Mann–Whitney test were used for parametric and non-parametric data, respectively. Ordinary 2- or 3-way ANOVA with Tukey's post hoc test was used for multiple comparisons. Significance is indicated in the box plots.

Results

Persistent inflammatory and innate immune response in PJI

Previous work in this *S. aureus* PJI model found elevated serum levels of acute-phase response protein serum amyloid A (SAA), a systemic marker of inflammation, and that infection was partially controlled but persistent, as the recovery of *S. aureus* CFUs decreased by 10-fold from 2 to 6 weeks.⁽²⁹⁾ We corroborated these results by finding a massive increase in serum SAA 1 week post infection, which diminished but remained elevated at the 5-week time point (Fig. 1A). A time course experiment revealed that serum SAA peaked 3 to 7 days post infection (dpi) and subsequently diminished by approximately 80% to an elevated plateau that was maintained at 14, 21, 28, and 35 dpi (Fig. 1B). The

SAA results are consistent with a persistent partially controlled infection. The transition to lower SAA levels corresponds to the timing of the emergence of an adaptive immune response.⁽⁴⁶⁾ The significantly higher levels of SAA even at 35 dpi compared with controls indicates a sustained inflammatory response in the setting of persistent infection.

To further investigate the sustained nature of the inflammatory and immune responses we performed a histological analysis of implanted knee joints (including tibiae and femora) of infected and non-infected control animals at multiple time points (3, 7, 14, 21 and 35 days) over a period of 5 weeks (Fig. 1C, representative photomicrographs). The amounts of tissue inflammation, necrosis, fibrotic tissue formation, and implant osseointegration were scored blindly by a pathologist (Fig. 1D) using a scoring system described in Supplemental Table S1. H&E-stained histological sections of operated limbs of non-infected mice revealed a mild inflammatory reaction at days 3 and 7, subsequently resolving over time in accord with our recent report.⁽⁴⁵⁾ In contrast, the tissues from infected animals had much more severe infiltration of inflammatory cells, mainly polymorphonuclear neutrophils (PMNs), as early as 3 dpi. At day 7, there was heavy acute inflammation involving intra-articular soft tissues, articular capsule, and surrounding soft tissues (Fig. 1E, top left). By day 21, diffuse large abscesses had formed, with massive tissue destruction, within and around the joint (Fig. 1C, lower row). Necrotizing granulomatous reactions surrounded by fibrotic sheets were observed at 21 and 35 dpi (Fig. 1C and 1E, top right). We also observed PMNs extending into the medullary canal starting at 7 dpi, and by day 35 there were necrotizing granulomas in the bone marrow, encapsulated by a fibrous band (Fig. 1E, bottom). Non-infected mice showed rapid and effective osseointegration, with multiple newly formed osseous trabeculae around the implant by day 7; in the infected tibiae, the ossification around the implant was initially delayed compared with the non-infected, and as the infection progressed to the medullary canal from the joint space, the new bone was resorbed by day 35. These results demonstrate infection that progresses from the joint space into the medullary canal beginning approximately 7 dpi and persists in the face of a sustained and extensive tissue inflammatory reaction.

Sustained infiltration of infected joint tissues by innate and adaptive immune cells

We used flow cytometry to perform a detailed and quantitative analysis of immune cells that infiltrate soft tissues of infected joints (the gating strategy and representative FACS plots are shown in Fig. 2A and Supplemental Fig. S1A, B). We compared day 7, corresponding to activation of adaptive immunity,⁽⁴⁷⁾ to day 35, corresponding to a more chronic phase of immune

Fig. 1. Persistent inflammatory and tissue-destructive response to *S. aureus* infection in a PJI mouse model. (A) Serum amyloid A levels in infected animals and uninfected controls at 7 and 35 dpi (*n* = 6/group per time point). (B) Serum amyloid A levels in non-infected controls and infected animals at the specified time points (*n* = 3/group per time point). Data are represented as median with interquartile range, two-way ANOVA followed by Tukey post hoc test. (C) Representative H&E-stained photomicrographs of knee joint sagittal sections of non-infected (top) controls and infected (bottom) animals at specified time points (*n* = 3/group per time point). (D) Histopathological scoring of H&E sections in (C). (E) Representative H&E-stained sections of infected mice at days 7 and 35 showing inflammation in the soft tissues around the joint and bone. (C) Scale bars = 400 μ m (top), 200 μ m (bottom). (E) Magnification $\times 10$, scale bars = 50 μ m. The images for control non-infected mice in (C) were derived from the same mice used in the study of Xia and colleagues,⁽⁴⁵⁾ and the scoring for control noninfected mice in (D) was performed on the same mice and samples as in the study of Xia and colleagues.⁽⁴⁵⁾ The control and infected mice were analyzed together as part of the same experiment.

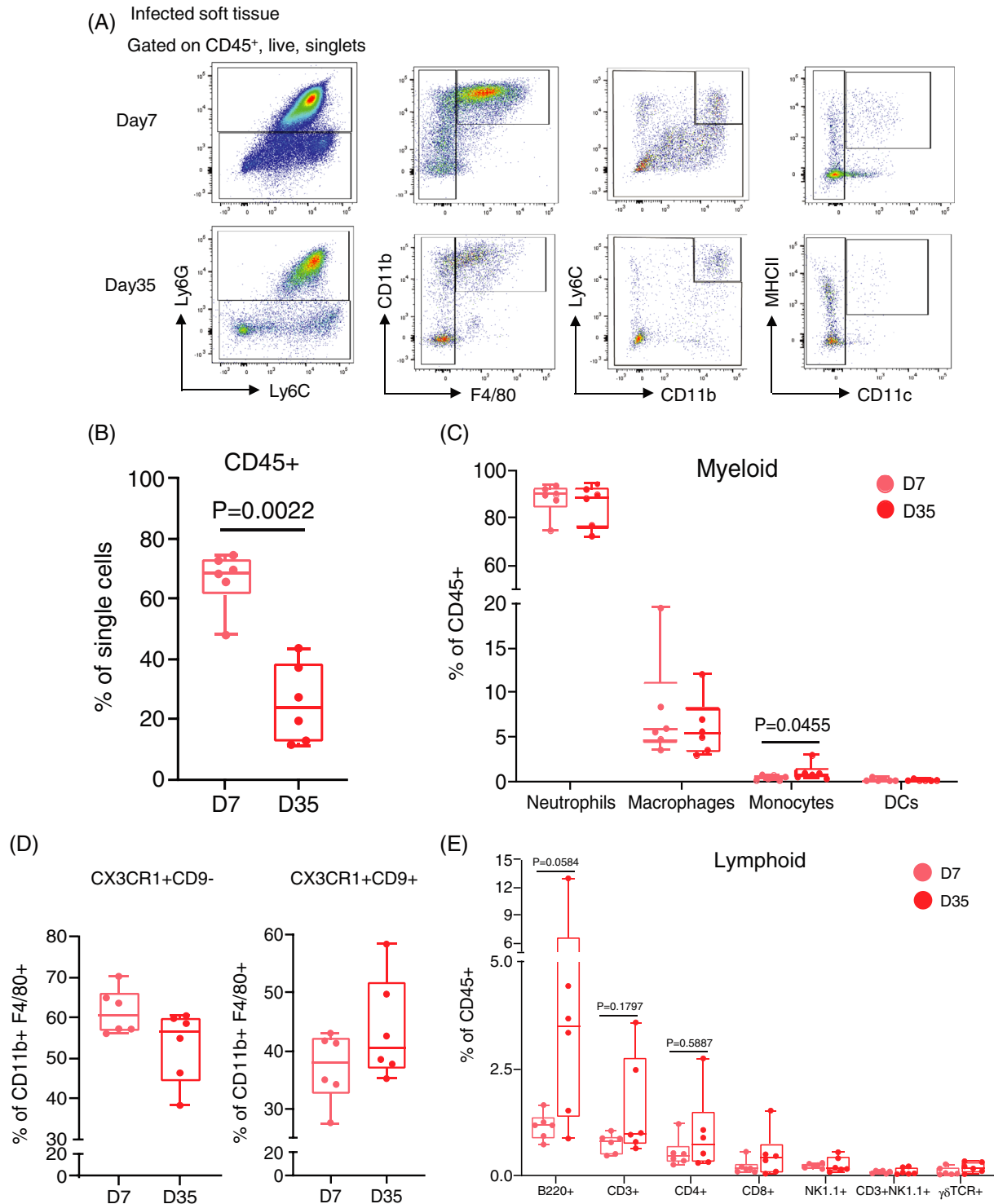


Fig. 2. Sustained infiltration of infected joint soft tissues by innate and adaptive immune cells. (A) Representative flow cytometric plots showing identification of myeloid populations in infected joint soft tissues at 7 and 35 dpi. (B) Frequency of CD45⁺ cells isolated from infected soft tissues at 7 and 35 dpi ($n = 6/\text{group}$ per time point). (C–E) Bar graphs of relative proportions of myeloid and lymphoid cell populations in infected joint soft tissues at 7 and 35 dpi ($n = 6/\text{group}$ per time point). Data are represented as median with interquartile range, Mann–Whitney test.

activity. Approximately 65% of the cells isolated from joint soft tissues were of hematopoietic origin (CD45⁺) at day 7, which decreased to ~25% by day 35 (Fig. 2B and Supplemental

Fig. 1C). As expected, neutrophils (Ly6G⁺Ly6C⁺ cells) were the dominant immune cell population (~80% of CD45⁺ cells) at day 7 (Fig. 2C); this predominance of neutrophils was sustained up

Soft tissue

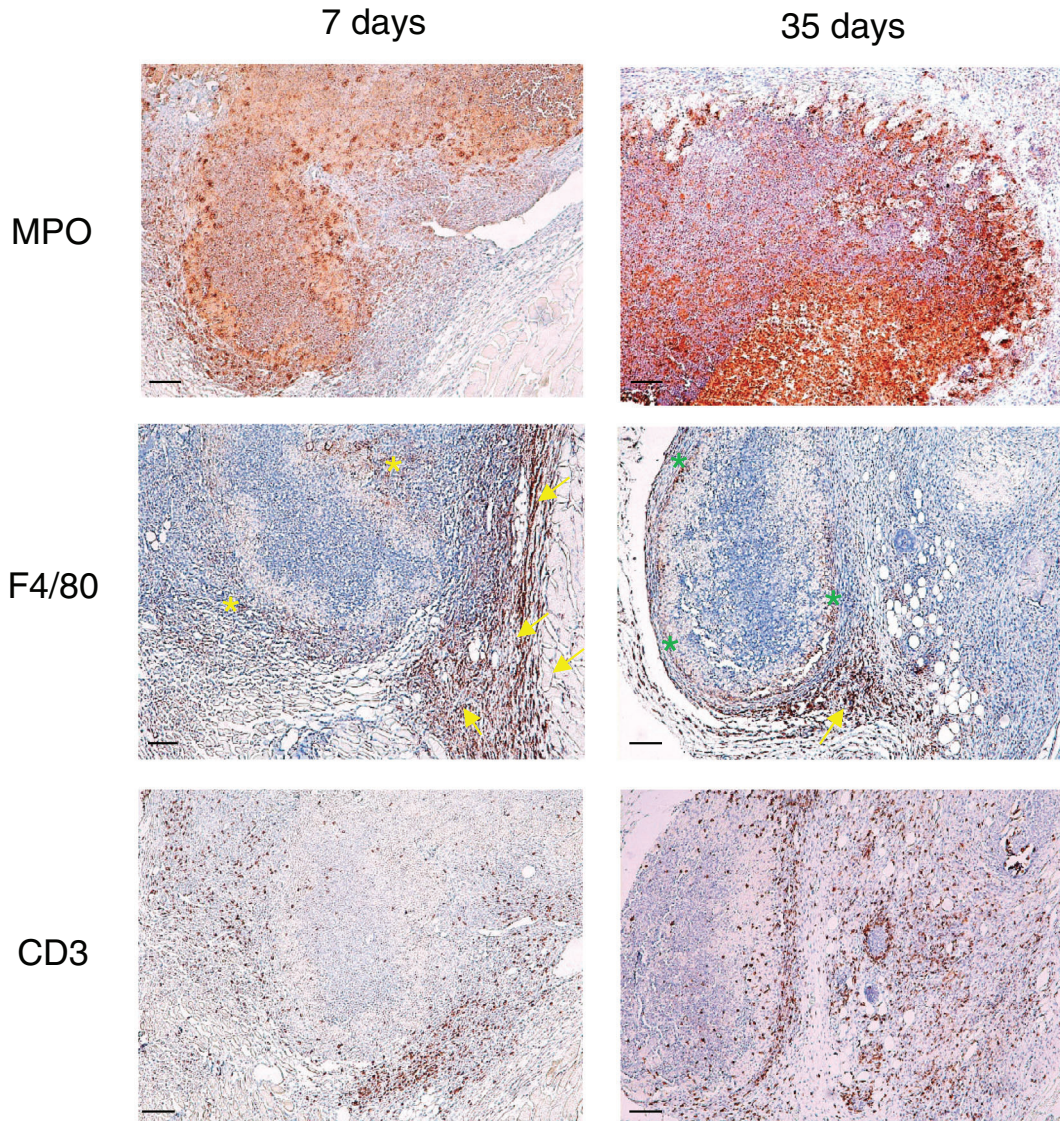


Fig. 3. Infiltration of infected joints by immune cells. Representative photomicrographs of immunohistochemical staining for MPO (neutrophils), F4/80 (macrophages), and CD3 (T cells) at 7 and 35 dpi ($n = 3/\text{group}$ per time point) in infected joint tissues (arrows = intensely F4/80 positive macrophages; yellow asterisks = larger macrophages with weaker F4/80 signal; green asterisks = macrophages around granulomas). Magnification $\times 10$; scale bars are $50 \mu\text{m}$.

to day 35. The cellular composition of other innate myeloid immune cells, $\text{CD11b}^+\text{F4/80}^+$ macrophages ($\sim 6\%$ of CD45^+ cells), $\text{CD11b}^+\text{Ly6C}^{\text{hi}}$ monocytes, and $\text{CD11c}^+\text{MHCII}^+$ dendritic cells, was also comparable on days 7 and 35 (Fig. 2C). Infiltrating macrophages were predominantly CX3CR1^+ , suggestive of a monocytic origin, and could be divided into CX3CR1 single-positive and $\text{CX3CR1}^+\text{CD9}^+$ double-positive macrophages (Supplemental Fig. S1A, upper right panel) whose relative proportions did not change substantially over time (Fig. 2D). Low levels of tissue infiltration by innate lymphocytes (NK cells, NKT cells, and $\gamma\delta$ T cells) did not change notably over time (Fig. 2E). Adaptive immune cells, namely B and T cells, represented a smaller fraction of immune infiltrates ($\sim 1\%$ to 2%) relative to myeloid

cells, but the proportion of lymphocytes in infected tissues was also sustained and comparable at 7 and 35 dpi (Fig. 2E).

We further corroborated and localized immune cell infiltration in infected tissues using immunohistochemistry to stain for MPO (myeloperoxidase, neutrophil marker), F4/80 (macrophage marker), and CD3 (T-cell marker) (Fig. 3 and Fig. S2 in Appendix S1). MPO staining showed a diffuse pattern throughout joint tissues in infected mice at both 7 and 35 dpi in comparison to the non-infected controls, with strong staining corresponding to abscesses, which may correspond to *Staphylococcus* abscess communities.^(27,42) At day 35, the MPO-positive areas were abundant in diaphyseal bone as well. F4/80-positive cells were found in the soft tissues around the joint, at both 7 and

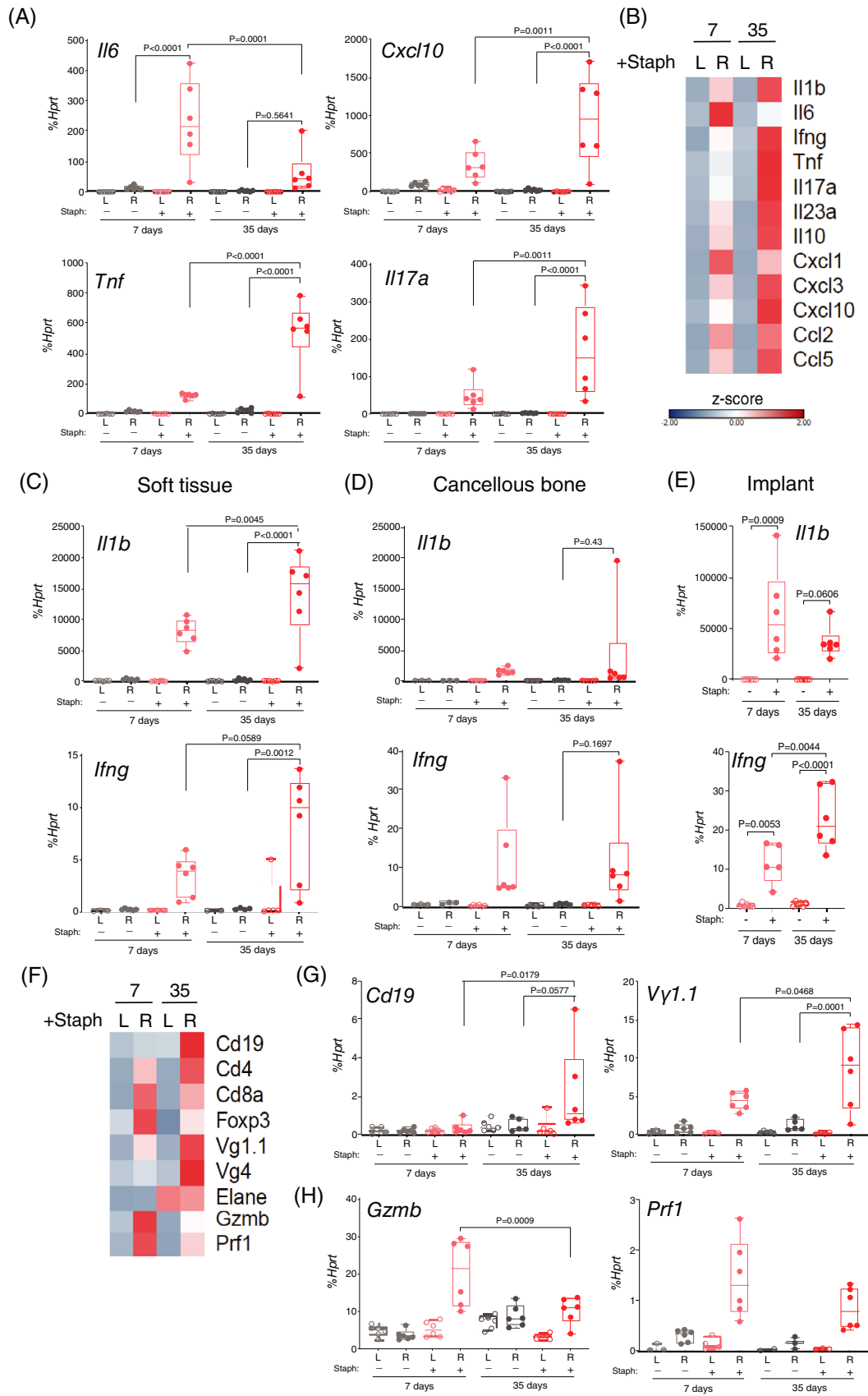


Fig. 4. Legend on next page.

35 days; intensely positive macrophages were abundant in the most superficial layers of capsule (arrows); bigger macrophages, with vacuolar cytoplasm and weaker F4/80 positivity, were located at the periphery of the abscesses at 7 days (yellow asterisks); at 35 days, this latter population was forming a more defined rim around the external wall of necrotizing granulomas (green asterisks). Infiltrating CD3⁺ T cells were found in the infected legs 7 dpi, especially in perivascular areas but also scattered through intra-articular and periarticular soft tissues. At day 35, T-cell staining remained similar and T cells were mostly concentrated around the edges of necrotizing granulomas in soft tissues and at the site around the implant. The non-infected legs showed only rare, scattered CD3⁺ cells (data not shown). Collectively, the data show sustained immune cell infiltration associated with persistent infection, with the cellular composition of the infiltrates not changing substantially over time.

Sustained activation of immune cells in infected tissues

To assess the activation status of immune cells in joint tissues post infection, we analyzed expression of innate and adaptive immune activation genes in infected and non-infected control animals 7 and 35 dpi by RT-qPCR. In accord with expected early activation of innate immunity, innate immune cell-expressed cytokine and chemokine genes such as *Il1b*, *Il6*, *Tnf*, *Il23a*, *Cxcl1*, *Cxcl3*, *Cxcl10*, and *Ccl5* were highly induced in infected joint tissues 7 dpi relative to control noninfected joint tissues (Fig. 4A–C). Expression of *Il6*, the major driver of SAA expression, declined from 7 to 35 dpi (Fig. 4A, B) in parallel with the decrease in SAA (Fig. 1A). Expression of a majority of the inflammatory/innate immune genes, including *Tnf*, *Il1b*, and Th17-promoting cytokine *Il23a*, and the neutrophil chemokines *Cxcl1* and *Cxcl3* was substantially and significantly increased on day 35 relative to 7 dpi. Interestingly, expression of major CD4⁺ T-cell effector genes *Ifng* (marker of a Th1 response that activates macrophages and targets intracellular bacteria) and *Il17a* (marker of a Th17 response that recruits PMNs and targets extracellular bacteria) was elevated 7 dpi and further increased by 35 dpi (Fig. 4A–C). Although PJI typically initiates in the joint tissues and adjacent implant, penetration of infection into the medullary canal and infection of bone (osteomyelitis) represents a catastrophic outcome.⁽¹⁾ Thus, we assessed immune gene activation in cells attached to the implant and in cancellous bone that more distally surrounds the implant. In line with histological findings showing infection of the medullary canal as early as 7 dpi, induction of both innate and adaptive immune genes at both sites was observed at both 7 and 35 dpi, although gene induction was less robust in the bone samples (Fig. 4D, E and Fig. S3 in Appendix S1). Collectively, these results show effective activation of innate and adaptive

immune cells in several infected tissues at 7 dpi, which persists or even increases at 35 dpi.

We also used this gene expression/qPCR approach to measure immune cell marker genes to corroborate the flow cytometry results; compared with flow cytometry where limiting cell numbers did not allow analysis of non-infected tissues, we were able to compare gene expression in infected versus noninfected tissues. Infected joint tissues exhibited increased expression of $\gamma\delta$ T-cell markers *Vg1.1* and *Vg4*, T-cell markers *Cd4* and *Cd8a*, and B-cell marker *Cd19* (Fig. 4F, G). Expression of *Cd19* and *Vg1.1* was significantly increased on day 35 relative to day 7 (Fig. 4G), whereas expression of the other cell marker genes did not significantly change with time. Interestingly, the CD8 T-cell effector genes *Gzmb* (encoding granzyme B) and *Prf1* (encoding perforin) were more highly expressed on day 7 than on day 35 (Fig. 4H). These results support infiltration of infected tissues by various immune cells and suggest that B cells accumulate at the later stages of infection, consistent with the trend for increased B cells observed by flow cytometry in Fig. 1.

Effects of CD8 T-cell depletion on PJI model

Increasing evidence suggests that *S. aureus* is not strictly an extracellular pathogen and can adapt to persist and divide intracellularly inside host cells, including in immune cells such as macrophages that have been termed “Trojan horses.”^(27,41) CD8⁺ cytotoxic lymphocytes are important for immunity against intracellular pathogens and could potentially be important in eradicating intracellularly infected joint or bone cells.⁽¹⁰⁾ The role of CD8⁺ T cells in immune responses to *S. aureus* is mostly unknown. As expression of CD8 T-cell effector genes that lyse infected target cells was elevated in our PJI model (Fig. 4), we tested the functional importance of CD8⁺ T cells using an antibody depletion strategy beginning 2 days before infection (Fig. S4 in Appendix S1 documents effectiveness of CD8⁺ T-cell depletion of >90%). Analysis of mice euthanized 17 dpi revealed that depletion of CD8⁺ T cells resulted in minimal and not statistically significant differences in serum SAA, joint histology, and joint tissue bacterial numbers (Fig. 5A–D). Gene expression analysis (Fig. 5E) confirmed depletion of CD8⁺ cells and also showed a moderate reduction in expression of *Ifng*, which encodes an important effector cytokine produced by CD8⁺ and CD4⁺ T cells. In line with lower *Ifng* expression, mRNA amounts encoded by IFN- γ -stimulated gene *Cxcl10* were significantly lower in CD8 T-cell-depleted mouse tissues (Fig. 5E). However, expression of various cytokine genes, including *Il17a*, *Tnf*, and *Il1b*, was not significantly different between the isotype and anti-CD8 α -treated groups. We conclude that CD8⁺ T cells play a minimal role in this PJI model.

Fig. 4. Immune cell activation and cytokine gene expression are maintained 35 dpi in infected joint tissues, cancellous bone, and peri-implant tissue. (A) qPCR analysis of the expression of *Il6*, *Cxcl10*, *Tnf*, and *Il17a* mRNA in joint soft tissues of non-infected and infected mice (RNA samples from the non-infected day 7 group in (A) and (C) are the same samples that were used in gene expression analysis in the study of Xia and colleagues.⁽⁴⁵⁾ (B) Heatmap of cytokine, chemokine, and immune effector molecule gene expression in joint soft tissues of infected mice at 7 and 35 dpi. (C–E) qPCR analysis of the expression of *Il1b* and *Ifng* mRNA in joint soft tissues (bilateral, L = left and R = right hind limbs), cancellous bones (bilateral, L = left and R = right hind limbs), and peri-implant tissue (operated right side only), respectively, of non-infected and infected mice at 7 and 35 dpi ($n = 6$ /group per time point; $n = 3$ for non-infected day 7 groups). (F) Heatmap of immune cell marker gene expression in joint soft tissues of infected mice at 7 and 35 dpi. (G) qPCR analysis of the expression of *Cd19*, *Vg4*, and (H) *Prf1* and *Gzmb* mRNA in joint soft tissues of non-infected and infected mice ($n = 6$ /group per time point; $n = 3$ for non-infected day 7 groups). Data are represented as median with interquartile range, three-way ANOVA followed by Tukey post hoc test.

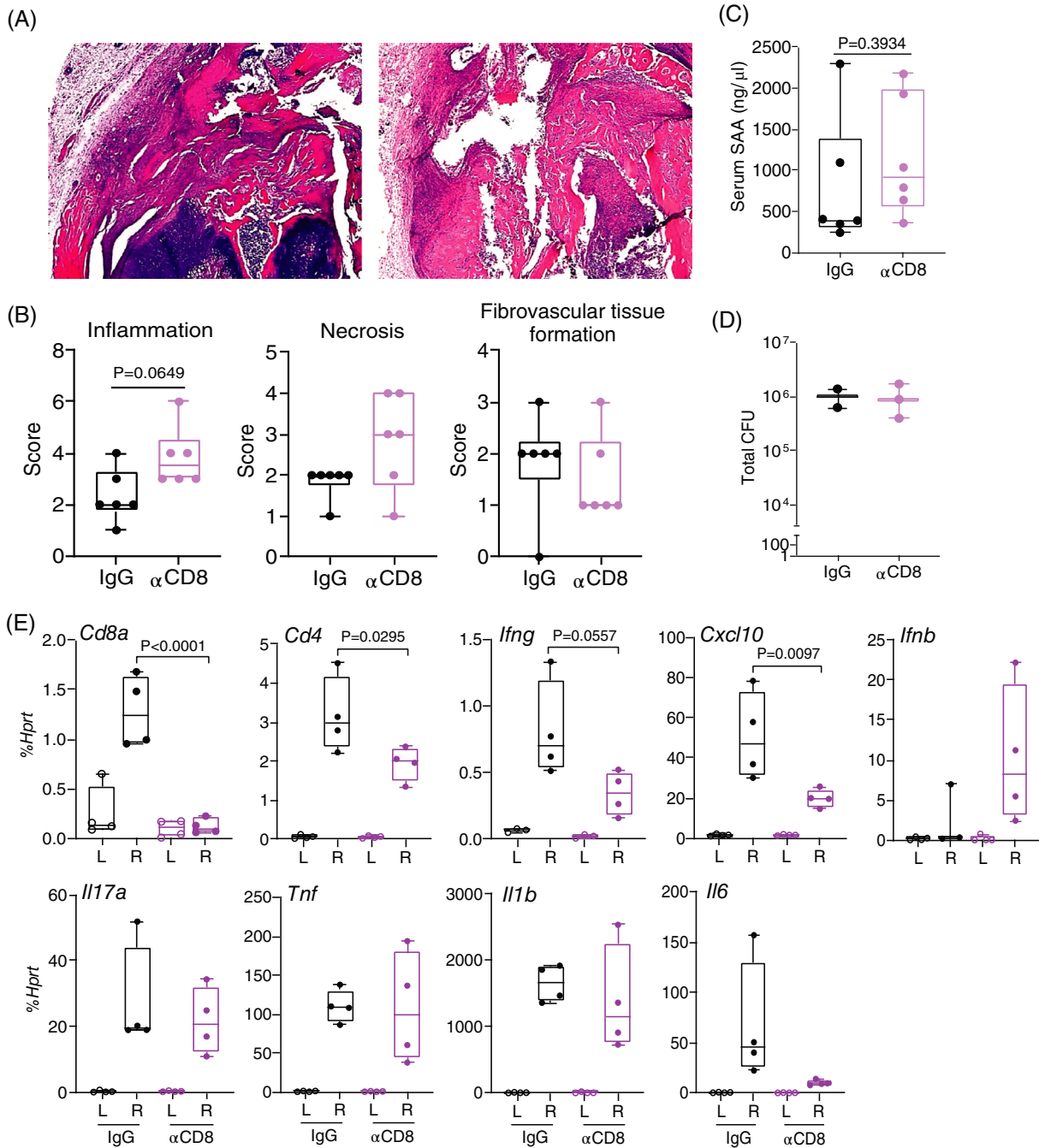


Fig. 5. Effects of CD8⁺ T-cell depletion on PJI. (A) Representative H&E-stained photomicrographs (magnification $\times 5$) of knee joint sagittal sections of isotype (left panel) and anti-CD8 (right panel) treated mice 17 dpi (data representative of two independent experiments, $n = 6$ /group). (B) Histopathological scoring of H&E sections in (A) ($n = 6$ /group). (C) Serum amyloid A levels and (D) total CFUs in the two groups of infected animals. Data are represented as median with interquartile range, Mann–Whitney test. (E) qPCR analysis of the expression of the specified genes in joint soft tissues (bilateral, L = left and R = right hind limbs) from isotype and anti-CD8-treated groups ($n = 4$ /group). Data are represented as median with interquartile range, two-way ANOVA followed by Tukey post hoc test.

Sustained mobilization of draining lymph nodes and bone marrow during PJI

Adaptive immunity is activated in draining LNs, where dendritic cells (DCs) that migrate from infected tissues present antigens to lymphocytes, which expand during active infection and subsequently contract after infection has been resolved. To evaluate whether activation of adaptive immunity is sustained at the later

phases of persistent PJI, we examined draining inguinal and iliac lymph nodes after surgery and infection. Infection resulted in a massive expansion of size and cellularity of iliac LNs that drain operated and infected joints (R, +) that was apparent at 7 dpi and was fully maintained at 35 dpi (Fig. 6A, B); similar but less pronounced increases were observed in draining inguinal LNs (Fig. S5 in Appendix S1). In line with our recent report,⁽⁴⁵⁾ surgery alone transiently expanded draining LNs at day 7, with a return

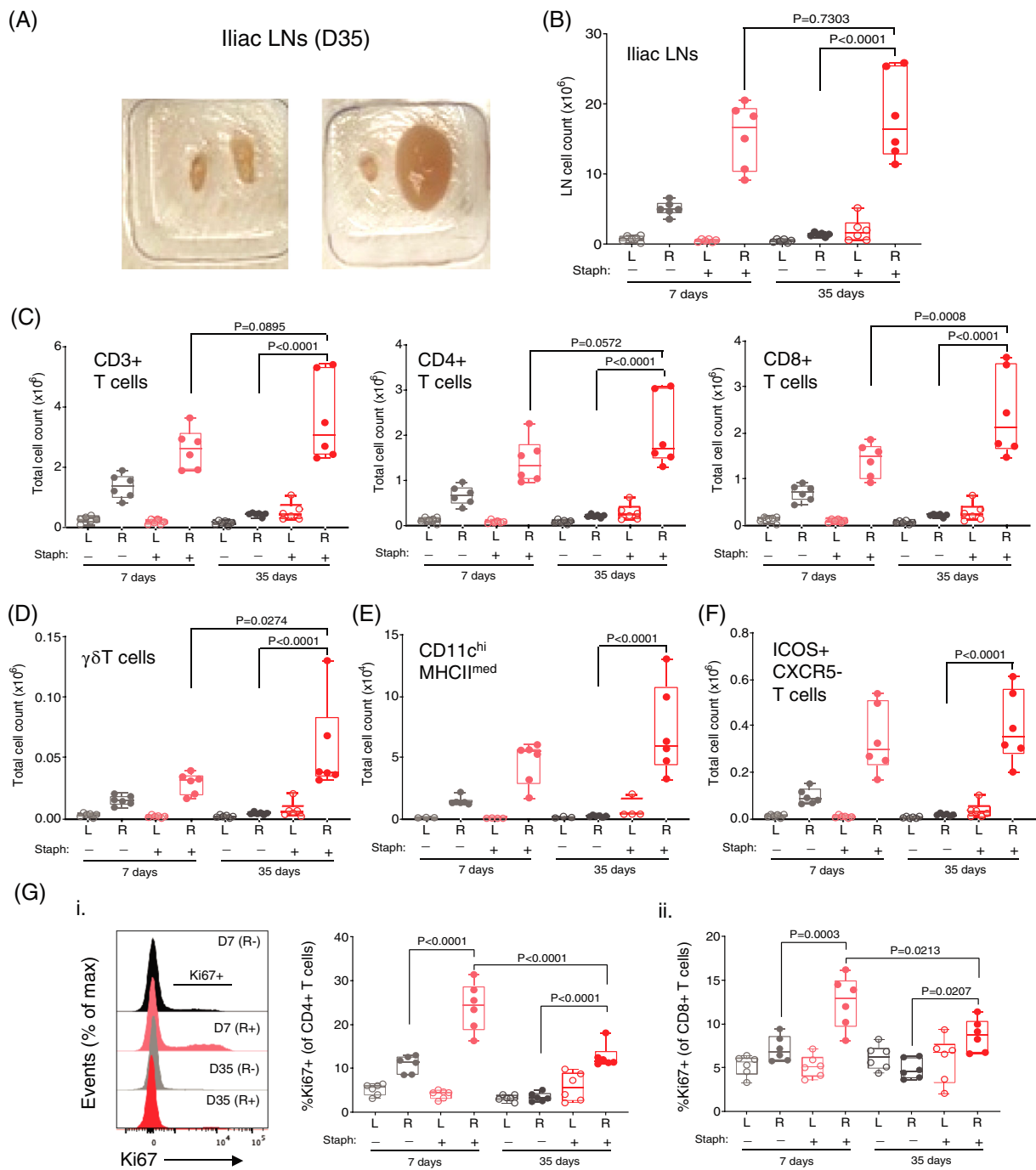


Fig. 6. Sustained expansion of draining iliac lymph nodes up to 35 dpi. (A) Representative photographs of iliac nodes harvested from non-infected (left panel) and infected (right panel) mice ($n = 3/\text{group}$ per time point) 35 dpi showing massive increase in size on the infected right side. Data representative of at least two independent experiments ($n = 6/\text{group}$ per time point). (B) Total cell counts of bilateral lymph nodes of non-infected and infected mice 7 and 35 dpi ($n = 6/\text{group}$ per time point). Total number of (C) CD3^+ , CD4^+ , and CD8^+ T cells, (D) $\text{TCR}\gamma\delta$ ($\text{CD3}^+\text{TCR}\gamma\delta^+$) T cells, (E) dendritic cells ($\text{CD11c}^{\text{hi}}\text{MHCII}^{\text{med}}$), and (F) $\text{CD3}^+\text{CD4}^+\text{ICOS}^+$ T cells, (G) proliferating (i) $\text{CD3}^+\text{CD4}^+$ T cells or (ii) $\text{CD3}^+\text{CD8}^+$ T cells as assessed by Ki67^+ staining of cells from iliac lymph nodes of non-infected and infected mice ($n = 6/\text{group}$ per time point) at 7 and 35 dpi. Data are represented as median with interquartile range, three-way ANOVA followed by Tukey post hoc test.

to near baseline at day 35. Substantial LN expansion was only observed on the infected R side, consistent with a unilateral infection.

Flow cytometric analysis (gating strategy shown in Fig. S6 in Appendix S1) showed pronounced accumulation of both CD4^+ and CD8^+ T cells in draining LNs 7 dpi and their numbers were

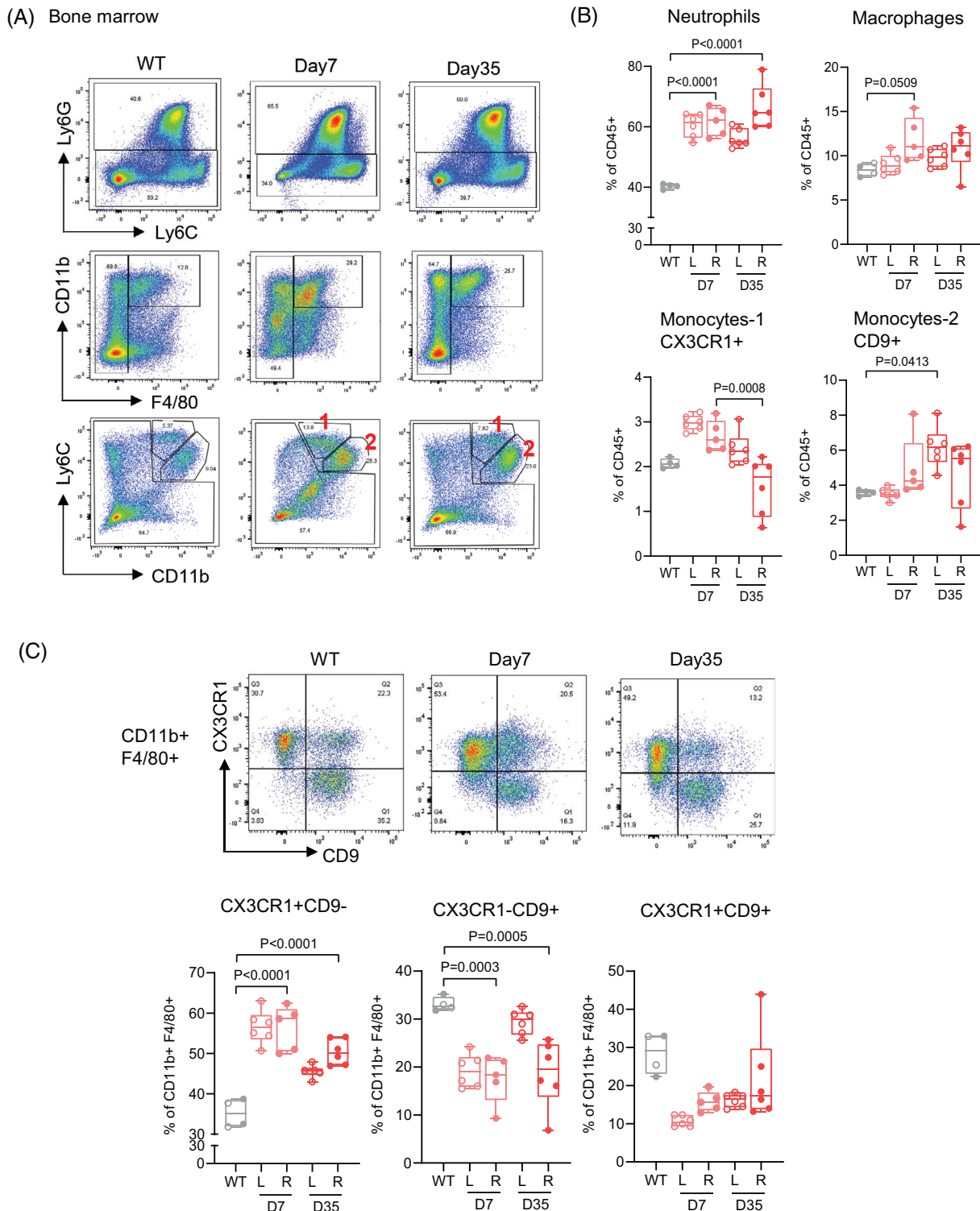


Fig. 7. Sustained bone marrow myeloid cell reaction post infection. (A) Representative flow cytometric plots showing identification of myeloid populations, (B) proportions of myeloid populations, and (C) expression of CD9 and CX3CR1 in CD11b⁺F4/80⁺ macrophages in bone marrows of naïve and infected mice at 7 and 35 dpi ($n = 4-6$ /group per time point; bilateral, L = left and R = right hind limbs). Data are represented as median with interquartile range, one-way ANOVA followed by Tukey post hoc test.

maintained or further increased at 35 dpi (Fig. 6C and Fig. S7 in Appendix S1). In accord with increased $\gamma\delta$ T cells in infected tissues at day 35, we observed increased numbers of $\gamma\delta$ T cells in

draining LNs at 35 dpi (Fig. 6D). Activation of T cells in LNs is mediated by dendritic cells (DCs) that migrate from infected tissues to present antigens in LNs. Accordingly, LNs draining

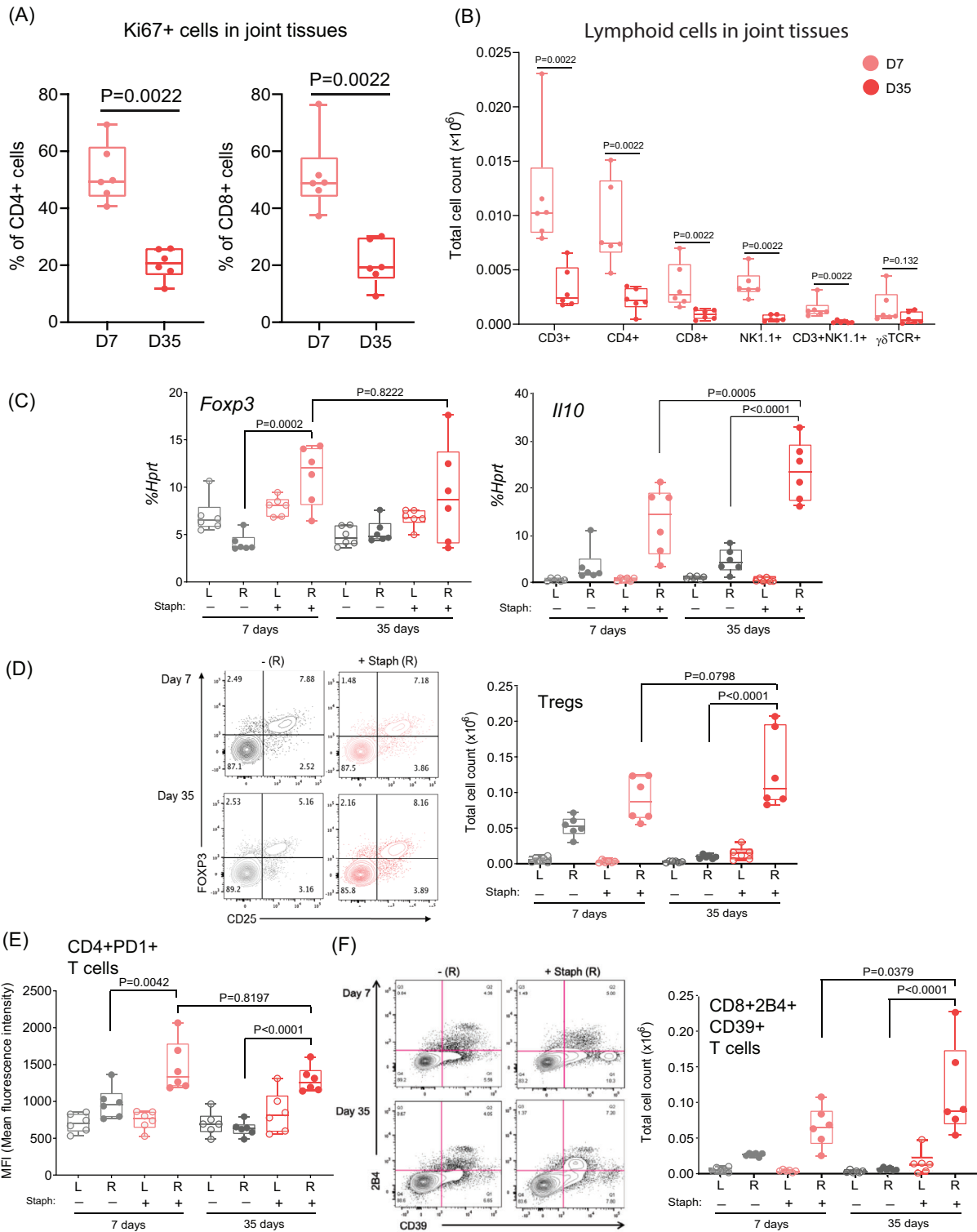


Fig. 8. Activation of feedback inhibitory pathways post infection. (A) Ki67 staining of proliferating CD4⁺ and CD8⁺ T cells in joint tissues ($n = 6$ /group per time point). (B) Absolute numbers of lymphoid cell populations in infected joint soft tissues at 7 and 35 dpi ($n = 6$ /group per time point). (C) qPCR analysis of the expression of *Foxp3* and *Il10* in joint soft tissues of infected mice at 7 and 35 dpi. (D) Total number of regulatory (CD3⁺CD4⁺CD25⁺Foxp3⁺) T cells in iliac lymph nodes of non-infected and infected mice 7 and 35 dpi. (E) Expression of PD-1 on CD4⁺ T cells. (F) Total number of CD8⁺2B4⁺CD39⁺ T cells in iliac lymph nodes from non-infected and infected animals 7 and 35 dpi as determined by flow cytometry ($n = 6$ /group per time point). Data are represented as median with interquartile range, three-way ANOVA followed by Tukey post hoc test.

infected joints harbored increased numbers of CD11c^{hi} MHCII^{int} DCs at both 7 and 35 dpi (Fig. 6E; gating strategy shown in Fig. S8A in Appendix S1). These LNs also exhibited increased numbers of neutrophils and monocytes (Fig. S8B in Appendix S1). An increased fraction of draining LN CD4⁺ T cells stained positive for activation marker ICOS at both 7 and 35 dpi (Fig. 6F); these ICOS⁺ T cells stained negative for CXCR5 (Fig. S6 in Appendix S1), suggesting they do not correspond to follicular helper T cells. In line with ongoing T-cell activation and related expansion in draining iliac LNs, approximately 25% of CD4⁺ and 13% of CD8⁺ T cells stained positive for the proliferation marker Ki67 at 7 dpi (Fig. 6G); the number of Ki67⁺ T cells in draining LNs diminished by day 35 but remained elevated relative to control LNs. Overall, these results support ongoing activation of T-cell immunity in draining LNs that persists through 35 days.

Infection mobilizes myelopoiesis in the bone marrow to generate neutrophils and monocytes that migrate to sites of infection.⁽⁴⁸⁾ In addition, as PJI extends into the medullary canal, *S. aureus* bacteria can directly activate myeloid cells in adjacent BM. We used flow cytometry to determine the effects of infection on neutrophils, monocytes, and macrophages in adjacent and contralateral tibial bone marrow; the gating strategy and representative FACS plots are shown in Fig. 7A and Fig. S1, Appendix S1. Relative to noninfected mice, infection substantially increased the fraction of Ly6G⁺ neutrophils in BM of infected mice on both the infected (right, R) and contralateral (left, L) sides, and this increase persisted from 7 to 35 dpi (Fig. 7B). Bone marrow macrophages were defined as CD11b⁺ F4/80⁺ (Fig. 7A) and three distinct populations were observed: CX3CR1 single-positive (CX3CR1⁺ CD9⁻), CD9 single-positive (CX3CR1⁻ CD9⁺), and CX3CR1⁺ CD9⁺ double-positive cells (Fig. 7C). Based on the expression pattern of Ly6C,⁽⁴⁹⁻⁵¹⁾ two distinct populations of monocytes were observed in the BM, CD11b⁺Ly6C^{hi} (Monocytes-1) and CD11b⁺Ly6C^{int} (Monocytes-2) (Fig. 7A). Monocytes-1 were CX3CR1⁺CD9⁻, whereas monocytes-2 were predominantly CX3CR1⁻CD9⁺ (Fig. S9 in Appendix S1). Similar to neutrophils, infection altered the relative numbers of the various macrophage and monocyte populations in both infected and contralateral tibias 7 and 35 dpi (Fig. 7B, C; Fig. S10 in Appendix S1 presents quantitation of the various cell populations). These results show that infection induces a myeloid lineage bone marrow reaction consistent with reactive myelopoiesis that occurs both in bone marrow adjacent to infection and distal bone marrow, and identify distinct monocyte and BM macrophage populations that can be distinguished based on CX3CR1 and CD9 expression.

Feedback inhibitory pathways that restrain immune responses

We investigated whether feedback inhibitory mechanisms that could restrain the tissue immune response were induced at 35 dpi. In accord with the activation phase of adaptive immunity on day 7, 50% of CD3⁺CD4⁺ and CD3⁺CD8⁺ T cells stained positive for the proliferation marker Ki67 (Fig. 8A). Strikingly, the fraction of Ki67⁺ T cells in infected tissues dramatically decreased from day 7 to day 35 post infection (Fig. 8A). When we calculated the total number of tissue-infiltrating T cells, correcting for cellularity (Fig. 2B and Fig. S1C in Appendix S1), both CD4⁺ and CD8⁺ T-cell numbers were markedly decreased in infected tissues on day 35 relative to day 7 post infection (Fig. 8B), despite maintenance of large numbers of T cells in draining LNs (Fig. 6).

Collectively, the results suggest that the LN and tissue T-cell responses are partially restrained by feedback inhibitory mechanisms, with a greater suppressive effect in infected tissues. In line with activation of inhibitory pathways, mRNA of the immune-suppressive cytokine IL-10 was significantly elevated in infected relative to non-infected tissues, and was higher at 35 dpi relative to 7 dpi (Fig. 8C). Expression of *Foxp3*, encoding the FOXP3 master regulator of regulatory T cells (Tregs), was also elevated in infected tissues (Fig. 8C), and higher numbers of Tregs that increased over time were observed in draining LNs (Fig. 8D). Finally, we measured T-cell surface expression of the inhibitory receptor PD1 that can restrain T-cell activation and of the exhaustion markers 2B4 and CD39.⁽⁴⁰⁾ CD4⁺ T cells in LNs draining infected tissues expressed significantly higher levels of PD1 (Fig. 8E), whereas a fraction of CD8⁺ T cells was double positive for 2B4 and CD39 (Fig. 8F), which corresponds to an exhausted functional phenotype.⁽⁴⁰⁾ Collectively, these results support the engagement of various feedback inhibitory pathways to restrain the immune response in an attempt to limit tissue damage and toxicity.

Discussion

The recalcitrance of orthopedic *S. aureus* PJI to antibiotic therapy highlights the importance of understanding immune responses to guide development of immunotherapies to help prevent and eradicate chronic PJI. In this study, we have defined immune responses and countervailing feedback mechanisms that restrain immunity in infected tissues, draining LNs and reactive bone marrow during early and persistent phases of PJI in a clinically relevant orthopedic model. Persistent infection is characterized by a sustained inflammatory reaction and strikingly high cytokine gene expression indicative of robust activation of multiple components of innate and adaptive immunity in infected joint and bone tissues. This tissue immune response is associated with and likely sustained by ongoing LN expansion and bone marrow reaction. However, feedback mechanisms involving inhibitory receptors, suppressive cytokines, and Tregs are operative during persistent infection and, together with sequestration of bacteria by encapsulation or biofilm, can contribute to failure of bacterial clearance. These findings identify a disconnect between ongoing immune activation in LNs and a “split tolerance” in infected tissues where inflammatory genes are highly expressed but cell proliferation and ability to clear infection are suppressed. The results suggest approaches to modulate the immune response to *S. aureus* PJI to promote eradication of infection in combination with debridement of biofilm and other therapeutic modalities.

In chronic infections with pathogens such as *Mycobacterium tuberculosis*, *Mycobacterium leprae*, HIV, or strains of LCMV, the host and pathogen reach a semi-stable state of equilibrium where the immune response becomes attenuated and infection is contained but not eliminated.^(39,40) The benefit to the host is avoidance of toxicity associated with cytokine storm and of extensive tissue damage associated with ongoing severe inflammation. In contrast, in *S. aureus* PJI, sustained high-level expression of immune activation genes, including cytokines and chemokines, is associated with ongoing high-grade inflammation, soft tissue destruction, and lysis of bone. Thus, the amount of inflammation required to contain *S. aureus* PJI is highly deleterious to the host and not particularly effective at clearing the pathogen. This raises the possibility that the immune response

to *S. aureus* PJI is “misdirected” and that activation of the innate immune, Th1, and Th17 pathways that we observed activates deleterious inflammatory pathways without engaging immune and microbicidal mechanisms that effectively clear *S. aureus* infection. Such skewed or maladaptive immune responses occur in other infections such as *M. Leprae*, and can be induced by the pathogen in order to escape the immune response.⁽⁵²⁾ Alternatively, the immune response may be appropriate, but *S. aureus* can disarm downstream effector mechanisms by various previously described mechanisms^(9,10,19) and thereby escape effective immunity.

Extensive investigation of *S. aureus* infection in the skin, the most common site of infection, has revealed that effective immunity is mediated by neutrophils, whose recruitment and function are amplified by inflammatory cytokines and type 3 IL-17-mediated immunity.^(14,16) In our PJI model, extensive neutrophil infiltration was associated with high-level cytokine, neutrophil chemoattractant, and IL-17 expression, but infection was not cleared. One possible explanation is that when *S. aureus* infection mobilizes the bone marrow, in addition to monocytes and neutrophils *S. aureus* strongly induces myeloid-derived suppressor cells (MDSCs).^(30,32,53-55) MDSCs are immature myeloid lineage cells related to monocytes or neutrophils that originate in the BM, follow a non-standard differentiation pathway, and infiltrate into infected tissues or tumors where they produce suppressive factors.^(56,57) Although best known as suppressors of T-cell responses, MDSCs also exhibit poor phagocytic capacity and produce anti-inflammatory cytokines, which would contribute to ineffectiveness at clearing *S. aureus*. Interestingly, in our *S. aureus* PJI model, we observed a strong myeloid BM reaction, with mobilization of cells expressing neutrophil markers and changes in the composition of monocyte and macrophage populations. We have followed consensus expert opinion that it is not possible to identify MDSCs based solely on currently known cell surface markers⁽⁵⁶⁾ and did not try to define MDSC populations within these myeloid cell populations based on cell surface phenotype. Instead, we have started to identify and define monocyte and macrophage subpopulations based on new cell surface markers such as CX3CR1 and CD9, with the goal of performing functional and gene expression analyses on purified cell populations in future work. CD9 appears to represent a promising marker as it clearly divides myeloid cells into subsets in our model, and CD9⁺ myeloid cells decrease in the BM while increasing in infected tissues over time. CD9⁺ macrophages can have pro-inflammatory and fibrotic phenotypes⁽⁵⁸⁻⁶⁰⁾ and it will be interesting to align CD9 subsets with inflammatory versus MDSC functions. Such an approach may identify new cell subpopulations and cell surface markers to selectively target to deplete suppressive myeloid cells, while preserving cell types important for host defense.

Although investigation of skin *S. aureus* infections and the genetics of susceptibility in children have highlighted the importance of the Th17-PMN axis in host defense, other immune mechanisms may be important, including humoral immunity⁽¹⁹⁾ and the IFN- γ -macrophage axis.^(10,23,24) Interestingly, children with defects in PMN function or Th17 responses outgrow their susceptibility to *S. aureus* infections, supporting the existence of alternative immune mechanisms that are effective against *S. aureus*.⁽¹⁶⁾ In this light, we investigated the role of CD8⁺ T cells. Although *S. aureus* is predominantly an extracellular pathogen, intracellular infection of various cell types, including osteoblasts and osteoclasts in PJI, has been described.^(10,61) An important component of the immune response against intracellular

pathogens is lysis of infected cells by cytotoxic lymphocytes (CTLs) that differentiate from CD8⁺ T cells. To our knowledge, the role of CTL-mediated killing in anti-*S. aureus* immunity has not been previously investigated but if effective could offer a potential strategy for immunotherapy. However, CD8⁺ T-cell depletion had minimal effects upon the course of PJI in our model, although expression of a subset of cytokines and ISGs was affected. Given that osteoblasts and osteoclasts are intracellularly infected by *S. aureus*, the most prominent effects of CD8⁺ T-cell depletion would be predicted to be on the bone component of infection. Thus, the effects of CD8 cell depletion may have been difficult to observe in our model, which has a strong soft tissue infection component similar to human PJI. We believe that it would be worthwhile to investigate the role of CD8⁺ T cells in an osteomyelitis model, where a greater proportion of cells may be intracellularly infected with *S. aureus*.

Attenuation of immune responses during chronic infection, and also the “exhaustion” of anti-tumor immune cells, have been primarily investigated at the site of infection or in the tumor.^(39,40) In infected tissues in our *S. aureus* PJI model, it is possible that activation of T-cell exhaustion markers may be due to polyclonal activation by superantigens such as staphylococcal enterotoxin B. Relatively little is known about how immunity is regulated in draining LNs in these chronic settings. In our PJI model, LN expansion and cellularity were maintained, if not increased, at 35 relative to 7 dpi, with increased numbers of DCs and expression of activation markers; although inhibitory receptor expression was elevated, lymphocyte proliferation was sustained at higher levels in LNs than in tissues. This indicates that immune responses were maintained in a more active state in draining LNs and then further downregulated, which can occur via suppression of migration of activated lymphocytes into infected tissues, and/or further suppression of cell activation in the tissues themselves. Our findings of relatively sparse tissue infiltration by T cells, on the order of 1% of CD45⁺ cells, is consistent with a report that T-cell infiltration in human PJI tissues is lower than in the low-grade inflammatory condition osteoarthritis.⁽⁶²⁾ Suppression of migration represents one of the mechanisms of action of Tregs, which together with MDSCs, can also suppress T-cell proliferation in infected tissues.

Immunotherapy with immune checkpoint blockade (ICB) that blocks the inhibitory receptors PD-1 and CTLA4 on T cells and activates immune-mediated rejection of tumors represents a major breakthrough in cancer therapy.^(39,40) Our findings and the PJI literature support developing immunotherapies that can be used in conjunction with debridement of biofilm and antibiotics to better control and possibly eradicate infections. Immunotherapy with anti-glucosaminidase antibodies has already been used successfully in combination with vancomycin in an orthopedic implant-associated osteomyelitis model,⁽²⁵⁾ establishing the utility of this approach. Given elevated expression of inhibitory receptors and exhaustion markers on CD4⁺ and CD8⁺ T cells in our PJI model, it would be reasonable to test ICB, although the limited role for CD8⁺ T cells that we have described limits enthusiasm for this approach. Our results support strategies that target Tregs and enhance migration of T cells into infected tissues, or target MDSCs to enhance immune cell expansion in infected tissues. Several strategies for eliminating MDSCs have shown promise in treatment of tumors and persistent infections including *S. aureus*,^(30,32) but a lack of specificity for MDSCs limits this approach.^(56,57) Given the phenotypic similarities of MDSCs to myeloid progenitors, monocytes, and neutrophils, there is also a concern that depleting MDSCs would

also deplete myeloid cells important for host defense. Instead, we suggest it may be fruitful to better understand pathways of MDSC differentiation in *S. aureus* PJI models and modulate these pathways to attenuate suppressor functions while strengthening antimicrobial mechanisms.

Our findings and potential strategies for immunotherapy need to be considered in the context of biofilm and other mechanical barriers, such as fibrin encapsulation, that sequester *S. aureus* in a sessile and quiescent form from immune cells. In orthopedic PJI, *S. aureus* can be sequestered in glycocalyx on implants and necrotic tissue, in abscess communities in the soft tissues and bone marrow, and within the canalicular network of the cortical bone.^(20,27) These sequestered bacteria detach and disperse into surrounding tissues and enter a planktonic phase, thus maintaining active infection, which drives inflammation/immunity and associated tissue damage. We have previously shown that biofilm forms in our model,⁽²⁹⁾ and the current data showing sustained high-level activation of inflammatory genes in infected tissues and of immune cells in draining lymph nodes support that the immune system is sensing late-phase infection, most like in a planktonic phase. Immunotherapy would be most effective in targeting the planktonic phase of infection and would need to be titrated to avoid overactivation of the immune system and to be used in combination with antibiotics and strategies that target or deplete biofilm. Antibiotic therapy will be incorporated in future studies and will help to model the phase of human PJI after antibiotic therapy is instituted subsequent to diagnosis, which can be delayed relative to initial symptoms of infection.

Our study has several limitations. Although we have made every effort to develop a clinically relevant PJI model^(28,29,63) and our findings are aligned with published studies of human PJI,^(62,64) it will be important to compare our findings to human PJI in greater detail. To this effect, we have initiated a study of human PJI subjects that to date has confirmed low-level T-cell infiltration, but greater heterogeneity and variability in duration of infection before surgical intervention will necessitate a long enrollment period. We did not directly assess the phagocytic, antimicrobial, and suppressive (MDSC) functions of tissue-infiltrating myeloid cells. This can be addressed in future work by sorting myeloid cells into subpopulations and performing functional studies, or alternatively by single-cell RNA sequencing.

In summary, we have identified a “split tolerance” in the immune response to *S. aureus* PJI where cell activation and cytokine production coexist with feedback inhibitory pathways that limit immunity but do not sufficiently suppress inflammation to prevent tissue damage. This work sets the stage for designing strategies to specifically modulate the immune response to promote eradication of infection.

Disclosures

The authors declare no conflicts of interest. LBI is a nonpaid consultant for Eli Lilly. MPB is a consultant and receives royalties from Smith and Nephew. AVC is a paid consultant for Heraeus.

Acknowledgments

We thank Orla O’Shea for tissue sectioning and histology, Theresa Lu and her laboratory staff (HSS) for advice about lymph node analysis and flow cytometry, and Weill Cornell Medicine–HSS Flow Cytometry Core Facility for flow cytometry support.

This work was supported by grants from the NIH (LBI) and by support for the Rosensweig Genomics Center from The Tow Foundation. The funding numbers are NIH R01 AI044938, R01 AR050401, and R01 DE019420.

Authors’ roles

UKS conceptualized, designed, and performed most of the experiments, prepared the figures, and wrote the manuscript. YX, BS, KT, and SNN contributed experiments. TP provided analysis of the histopathology. MPB, AVC, and XY contributed expertise and intellectual input. XY performed surgeries with assistance from UKS, YX, and SNN. LBI conceptualized and oversaw the study and edited the manuscript. All authors reviewed and provided input on the manuscript.

Data availability statement

All the data are available within the article or its supplemental materials.

References

1. Ricciardi BF, Muthukrishnan G, Masters EA, Kaplan N, Daiss JL, Schwarz EM. New developments and future challenges in prevention, diagnosis, and treatment of prosthetic joint infection. *J Orthop Res.* 2020;38(7):1423-1435.
2. Tande AJ, Patel R. Prosthetic joint infection. *Clin Microbiol Rev.* 2014; 27(2):302-345.
3. Scherr TD, Heim CE, Morrison JM, Kielian T. Hiding in plain sight: interplay between staphylococcal biofilms and host immunity. *Front Immunol.* 2014;5:37.
4. Weiser MC, Moucha CS. The current state of screening and decolonization for the prevention of *Staphylococcus aureus* surgical site infection after total hip and knee arthroplasty. *J Bone Joint Surg Am.* 2015;97(17):1449-1458.
5. Kim MK, Zhao A, Wang A, et al. Surface-attached molecules control *Staphylococcus aureus* quorum sensing and biofilm development. *Nat Microbiol.* 2017;2:17080.
6. Costerton JW, Stewart PS, Greenberg EP. Bacterial biofilms: a common cause of persistent infections. *Science (New York, NY).* 1999; 284(5418):1318-1322.
7. Urish KL, DeMuth PW, Craft DW, Haider H, Davis CM 3rd. Pulse lavage is inadequate at removal of biofilm from the surface of total knee arthroplasty materials. *J Arthroplasty.* 2014;29(6):1128-1132.
8. Goswami K, Cho J, Foltz C, et al. Polymyxin and bacitracin in the irrigation solution provide no benefit for bacterial killing in vitro. *J Bone Joint Surg Am.* 2019;101(18):1689-1697.
9. Goldmann O, Medina E. *Staphylococcus aureus* strategies to evade the host acquired immune response. *Int J Med Microbiol.* 2018; 308(6):625-630.
10. Bröker BM, Mrochen D, Péton V. The T cell response to *Staphylococcus aureus*. *Pathogens (Basel, Switzerland).* 2016;5(1):31.
11. de Vor L, Rooijackers SHM, van Strijp JAG. *Staphylococci* evade the innate immune response by disarming neutrophils and forming biofilms. *FEBS Lett.* 2020;594(16):2556-2569.
12. Clegg J, Soldaini E, McLoughlin RM, Rittenhouse S, Bagnoli F, Phogat S. *Staphylococcus aureus* vaccine research and development: the past, present and future, including novel therapeutic strategies. *Front Immunol.* 2021;12:705360.
13. Miller LS, Fowler VG, Shukla SK, Rose WE, Proctor RA. Development of a vaccine against *Staphylococcus aureus* invasive infections: evidence based on human immunity, genetics and bacterial evasion mechanisms. *FEMS Microbiol Rev.* 2020;44(1):123-153.
14. Miller LS, Cho JS. Immunity against *Staphylococcus aureus* cutaneous infections. *Nat Rev Immunol.* 2011;11(8):505-518.

15. Metzemaekers M, Gouwy M, Proost P. Neutrophil chemoattractant receptors in health and disease: double-edged swords. *Cell Mol Immunol.* 2020;17(5):433-450.
16. Maródi L, Cypowjy S, Tóth B, Chernyshova L, Puel A, Casanova JL. Molecular mechanisms of mucocutaneous immunity against *Candida* and *Staphylococcus* species. *J Allergy Clin Immunol.* 2012; 130(5):1019-1027.
17. Marchitto MC, Dillen CA, Liu H, et al. Clonal V γ 6(+)/V δ 4(+) T cells promote IL-17-mediated immunity against *Staphylococcus aureus* skin infection. *Proc Natl Acad Sci USA.* 2019;116(22):10917-10926.
18. Chan LC, Chaili S, Filler SG, et al. Nonredundant roles of interleukin-17A (IL-17A) and IL-22 in murine host defense against cutaneous and hematogenous infection due to methicillin-resistant *Staphylococcus aureus*. *Infect Immun.* 2015;83(11):4427-4437.
19. Karauzum H, Datta SK. Adaptive immunity against *Staphylococcus aureus*. *Curr Top Microbiol Immunol.* 2017;409:419-439.
20. Saeed K, McLaren AC, Schwarz EM, et al. 2018 International Consensus Meeting on Musculoskeletal Infection: summary from the biofilm workgroup and consensus on biofilm related musculoskeletal infections. *J Orthop Res.* 2019;37(5):1007-1017.
21. Saeed K, Sendi P, Arnold WV, et al. Bacterial toxins in musculoskeletal infections. *J Orthop Res.* 2021;39(2):240-250.
22. Ricciardi BF, Muthukrishnan G, Masters E, Ninomiya M, Lee CC, Schwarz EM. *Staphylococcus aureus* evasion of host immunity in the setting of prosthetic joint infection: biofilm and beyond. *Curr Rev Musculoskelet Med.* 2018;11(3):389-400.
23. Brown AF, Murphy AG, Lalor SJ, et al. Memory Th1 cells are protective in invasive *Staphylococcus aureus* infection. *PLoS Pathog.* 2015; 11(11):e1005226.
24. Barin JG, Talor MV, Schaub JA, et al. Collaborative interferon- γ and interleukin-17 signaling protects the oral mucosa from *Staphylococcus aureus*. *Am J Pathol.* 2016;186(9):2337-2352.
25. Yokogawa N, Ishikawa M, Nishitani K, et al. Immunotherapy synergizes with debridement and antibiotic therapy in a murine 1-stage exchange model of MRSA implant-associated osteomyelitis. *J Orthop Res.* 2018;36(6):1590-1598.
26. Otto M. *Staphylococcus aureus* toxins. *Curr Opin Microbiol.* 2014;17: 32-37.
27. Masters EA, Trombetta RP, de Mesy Bentley KL, et al. Evolving concepts in bone infection: redefining "biofilm," "acute vs. chronic osteomyelitis," "the immune proteome" and "local antibiotic therapy". *Bone Res.* 2019;7:20.
28. Carli AV, Ross FP, Bhimani SJ, Nodzo SR, Bostrom MP. Developing a clinically representative model of periprosthetic joint infection. *J Bone Joint Surg Am.* 2016;98(19):1666-1676.
29. Carli AV, Bhimani S, Yang X, et al. Quantification of peri-implant bacterial load and in vivo biofilm formation in an innovative, clinically representative mouse model of periprosthetic joint infection. *J Bone Joint Surg Am.* 2017;99(6):e25.
30. Tebartz C, Horst SA, Sparwasser T, et al. A major role for myeloid-derived suppressor cells and a minor role for regulatory T cells in immunosuppression during *Staphylococcus aureus* infection. *J Immunol (Baltimore, MD: 1950).* 2015;194(3):1100-1111.
31. Aldrich AL, Heim CE, Shi W, Fallet RW, Duan B, Kielian T. TLR2 and caspase-1 signaling are critical for bacterial containment but not clearance during craniotomy-associated biofilm infection. *J Neuroinflammation.* 2020;17(1):114.
32. Heim CE, Vidlak D, Scherr TD, et al. Myeloid-derived suppressor cells contribute to *Staphylococcus aureus* orthopedic biofilm infection. *J Immunol.* 2014;192(8):3778-3792.
33. Brady RA, Mocca CP, Plaut RD, Takeda K, Burns DL. Comparison of the immune response during acute and chronic *Staphylococcus aureus* infection. *PLoS One.* 2018;13(3):e0195342.
34. Ziegler C, Goldmann O, Hobeika E, Geffers R, Peters G, Medina E. The dynamics of T cells during persistent *Staphylococcus aureus* infection: from antigen-reactivity to in vivo anergy. *EMBO Mol Med.* 2011;3(11):652-666.
35. Li D, Gromov K, Søballe K, et al. Quantitative mouse model of implant-associated osteomyelitis and the kinetics of microbial growth, osteolysis, and humoral immunity. *J Orthop Res.* 2008; 26(1):96-105.
36. Niska JA, Meganck JA, Pribaz JR, et al. Monitoring bacterial burden, inflammation and bone damage longitudinally using optical and μ CT imaging in an orthopaedic implant infection in mice. *PLoS One.* 2012;7(10):e47397.
37. Prabhakara R, Harro JM, Leid JG, Harris M, Shirtliff ME. Murine immune response to a chronic *Staphylococcus aureus* biofilm infection. *Infect Immun.* 2011;79(4):1789-1796.
38. Wang Y, Ashbaugh AG, Dikeman DA, et al. Interleukin-1 β and tumor necrosis factor are essential in controlling an experimental orthopedic implant-associated infection. *J Orthop Res.* 2020;38(8):1800-1809.
39. McLane LM, Abdel-Hakeem MS, Wherry EJ. CD8 T cell exhaustion during chronic viral infection and cancer. *Annu Rev Immunol.* 2019;37: 457-495.
40. Philip M, Schietinger A. Heterogeneity and fate choice: T cell exhaustion in cancer and chronic infections. *Curr Opin Immunol.* 2019;58: 98-103.
41. Nishitani K, Ishikawa M, Morita Y, et al. IsdB antibody-mediated sepsis following *S. aureus* surgical site infection. *JCI Insight.* 2020;5(19): e141164.
42. Thammavongsa V, Missiakas DM, Schneewind O. *Staphylococcus aureus* degrades neutrophil extracellular traps to promote immune cell death. *Science (New York, NY).* 2013;342(6160):863-866.
43. Carli AV, Bhimani S, Yang X, de Mesy Bentley KL, Ross FP, Bostrom MP. Vancomycin-loaded polymethylmethacrylate spacers fail to eradicate periprosthetic joint infection in a clinically representative mouse model. *J Bone Joint Surg Am.* 2018;100(11):e76.
44. Yang X, Ricciardi BF, Dvorzhinskiy A, et al. Intermittent parathyroid hormone enhances cancellous osseointegration of a novel murine tibial implant. *J Bone Joint Surg Am.* 2015;97(13):1074-1083.
45. Xia Y, Sokhi UK, Bell RD, et al. Immune and repair responses in joint tissues and lymph nodes after knee arthroplasty surgery in mice. *J Bone Miner Res.* 2021;36(9):1765-1780.
46. De Buck M, Gouwy M, Wang JM, et al. The cytokine-serum amyloid A-chemokine network. *Cytokine Growth Factor Rev.* 2016;30:55-69.
47. Sette A, Trotta S. Adaptive immunity to SARS-CoV-2 and COVID-19. *Cell.* 2021;184(4):861-880.
48. Mitroulis I, Kalafati L, Bornhäuser M, Hajishengallis G, Chavakis T. Regulation of the bone marrow niche by inflammation. *Front Immunol.* 2020;11:1540.
49. Gordon S, Taylor PR. Monocyte and macrophage heterogeneity. *Nat Rev Immunol.* 2005;5(12):953-964.
50. Clements M, Gershenovich M, Chaber C, et al. Differential Ly6C expression after renal ischemia-reperfusion identifies unique macrophage populations. *J Am Soc Nephrol.* 2016;27(1):159-170.
51. Shi C, Velázquez P, Hohl TM, Leiner I, Dustin ML, Pamer EG. Monocyte trafficking to hepatic sites of bacterial infection is chemokine independent and directed by focal intercellular adhesion molecule-1 expression. *J Immunol (Baltimore, MD: 1950).* 2010;184(11):6266-6274.
52. Modlin RL. Th1-Th2 paradigm: insights from leprosy. *J Invest Dermatol.* 1994;102(6):828-832.
53. Heim CE, Vidlak D, Kielian T. Interleukin-10 production by myeloid-derived suppressor cells contributes to bacterial persistence during *Staphylococcus aureus* orthopedic biofilm infection. *J Leukoc Biol.* 2015;98(6):1003-1013.
54. Aldrich AL, Horn CM, Heim CE, Korshoj LE, Kielian T. Transcriptional diversity and niche-specific distribution of leukocyte populations during *Staphylococcus aureus* craniotomy-associated biofilm infection. *J Immunol (Baltimore, MD: 1950).* 2021;206(4):751-765.
55. Heim CE, West SC, Ali H, Kielian T. Heterogeneity of Ly6G(+) Ly6C(+) myeloid-derived suppressor cell infiltrates during *Staphylococcus aureus* biofilm infection. *Infect Immun.* 2018;86(12):e00684.
56. Bronte V, Brandau S, Chen SH, et al. Recommendations for myeloid-derived suppressor cell nomenclature and characterization standards. *Nat Commun.* 2016;7:12150.
57. Veglia F, Sanseviero E, Gabrilovich DI. Myeloid-derived suppressor cells in the era of increasing myeloid cell diversity. *Nat Rev Immunol.* 2021;21(8):485-498.

58. Hill DA, Lim HW, Kim YH, et al. Distinct macrophage populations direct inflammatory versus physiological changes in adipose tissue. *Proc Natl Acad Sci USA*. 2018;115(22):E5096-E5105.
59. Jaitin DA, Adlung L, Thaiss CA, et al. Lipid-associated macrophages control metabolic homeostasis in a Trem2-dependent manner. *Cell*. 2019;178(3):686-98.e14.
60. Ramachandran P, Dobie R, Wilson-Kanamori JR, et al. Resolving the fibrotic niche of human liver cirrhosis at single-cell level. *Nature*. 2019;575(7783):512-518.
61. Krauss JL, Roper PM, Ballard A, et al. *Staphylococcus aureus* infects osteoclasts and replicates intracellularly. *MBio*. 2019;10(5):e02447-e02419.
62. Heim CE, Vidlak D, Odvody J, Hartman CW, Garvin KL, Kielian T. Human prosthetic joint infections are associated with myeloid-derived suppressor cells (MDSCs): implications for infection persistence. *J Orthop Res*. 2018;36(6):1605-1613.
63. Sosa BR, Niu Y, Turajane K, et al. John Charnley Award: the antimicrobial potential of bacteriophage-derived lysin in a murine debridement, antibiotics, and implant retention model of prosthetic joint infection. *Bone Joint J*. 2020;102(7B):3-10.
64. Korn MF, Stein RR, Dolf A, et al. High-dimensional analysis of immune cell composition predicts periprosthetic joint infections and dissects its pathophysiology. *Biomedicine*. 2020;8(9):358.